DØ Note 4722-CONF

Improved Search for Single Top Quark Production at DØ in Run II

The DØ Collaboration
http://www-d0.fnal.gov
(Dated: March 31, 2005)

We present a search for electroweak production of single top quarks in the s-channel and t-channel modes. We have analyzed 230 pb^{-1} of data collected with the DØ detector at the Fermilab Tevatron collider at a center-of-mass energy of $\sqrt{s} = 1.96$ TeV. Three separate analysis methods are used: neural networks, decision trees and a cut-based analysis. No evidence for a single top signal is found. We set 95% confidence level Bayesian upper limits on the production cross sections using binned likelihood fits to the neural network and decision tree output distributions and using the total numbers of events in the cut-based analysis. The limits from the neural networks (decision trees, cut-based) analysis are 6.4 pb (8.3 pb, 10.6 pb) in the s-channel and 5.0 pb (8.1 pb, 11.3 pb) in the t-channel.

Preliminary Results for Winter 2005 Conferences

I. INTRODUCTION

Top quark physics offers insight into fundamental aspects of the standard model, both in the strong and electroweak sectors. The top quark was discovered in 1995 at the Fermilab Tevatron collider in $t\bar{t}$ events produced via the strong interaction [1]. The standard model predicts that proton-antiproton collisions should also produce single top quarks through electroweak interactions. Studying single top quark production will provide information on the CKM matrix element $|V_{tb}|$, the top quark polarization, and will probe possible new physics in the top quark sector. There are two dominant modes of single top quark production: the s-channel process $p\overline{p} \to t\overline{b} + X$ and the t-channel process $p\overline{p} \to tq\overline{b} + X$. The production cross sections have been calculated at next-to-leading order (NLO) in the strong coupling [2–4]. The predicted cross sections for $M_t = 175$ GeV and $\sqrt{s} = 1.96$ TeV are 0.88 ± 0.14 pb and 1.98 ± 0.30 pb [2], respectively. Both the DØ and CDF collaborations have performed searches for single top quark production in Run I [5–7]. At the 95% confidence level, the DØ limit on the s-channel is 17 pb, and the CDF limit is 18 pb. At the same confidence level, the limit on the t-channel production cross section is 22 pb from DØ and 13 pb from CDF. CDF has also completed a search in Run II and placed upper limits on the production cross sections of 13.6 pb (s-channel), 10.1 pb (t-channel), and 17.8 pb (s+t combined) [8].

In this note, we use the notation "tb" to include both $t\bar{b}$ and the charge conjugate process $\bar{t}b$, and "tqb" to include both $tq\bar{b}$ and $\bar{t}\bar{q}b$.

This analysis focuses on the final state topology of single top quark production where the top quark decays into a b quark and a W boson, which subsequently decays leptonically ($W \to e\nu,\ \mu\nu$). This gives rise to an event signature with a high transverse momentum lepton, and significant missing transverse energy from the neutrino, in association with up to two b quark jets (with an additional light-quark jet in t-channel production). The largest backgrounds to this event signature come from W+jets and $t\bar{t}$ production.

The analysis proceeds as follows. We select signal-like events and separate the data into independent analysis sets based on final state lepton flavor (electron or muon) and b-tag multiplicity (=1 tag and ≥2 tags), where b quark jets are tagged using reconstructed displaced vertices in the jets. The independent analysis sets are combined in the final statistical analysis. We apply three analysis methods: a cut-based selection, and two multivariate analyses using neural networks and decision trees to separate the signals from the large backgrounds. Binned likelihood fits are performed on the neural network and decision tree outputs to obtain cross section limits.

II. THE DØ DETECTOR

The DØ detector in Run II consists of a central tracking system, a liquid-argon/uranium calorimeter, and an iron toroid muon spectrometer [9]. The central tracking system includes a silicon microstrip tracker and a central fiber tracker, both located within a 2 T superconducting solenoidal magnet. The calorimeters consist of a central module covering the detector pseudorapidity region $|\eta_{\rm det}| < 1.1$ and two end calorimeters extending the coverage to $|\eta_{\rm det}| < 4.2$. The muon system resides outside the calorimeter, and consists of a layer of tracking detectors and scintillation counters before 1.8 T toroids, followed by two similar layers after the toroids.

III. DATA AND EVENT SELECTION

The analysis is based on inclusive electron and muon data recorded between August 2002 and March 2004. The data were collected using a trigger that required an electromagnetic energy cluster and a jet in the calorimeter for the electron channel, and a muon and a jet for the muon channel. The integrated luminosity is 226 ± 15 pb^{-1} for the electron channel and 229 ± 15 pb^{-1} for the muon channel.

In the electron channel, candidate events are selected by requiring exactly one isolated electron (based on a seven-variable likelihood) with $E_T > 15$ GeV and $|\eta_{\rm det}| < 1.1$. In the muon channel, events are selected by requiring exactly one isolated muon with $p_T > 15$ GeV and $|\eta_{\rm det}| < 2.0$. For both channels, the events are also required to have missing transverse energy $\not\!\!E_T > 15$ GeV. Events must have between two and four jets with the leading jet $E_T > 25$ GeV and $|\eta_{\rm det}| < 2.5$, and the additional jets having $E_T > 15$ GeV and $|\eta_{\rm det}| < 3.4$. Misreconstructed events are rejected by requiring that low $\not\!\!E_T$ is not aligned or anti-aligned with leptons or jets. We require at least one b-tagged jet, and separate the s-channel from the t-channel search by requiring at least one non b-tagged jet in the t-channel analysis.

Secondary-vertex tagging is used to identify displaced vertices of long-lived particles like those from B hadrons. To form secondary vertices, charged tracks are selected on the basis of the significance of their distance of closest approach (X_{dca}) to the primary vertex. Tracks are first grouped in cones of radius $R = \sqrt{(\Delta\eta)^2 + (\Delta\phi)^2} = 0.5$ around a seed track with $p_T > 1$ GeV and $X_{dca}/\sigma_{X_{dca}} > 3.5$, where $\sigma_{X_{dca}}$ is the uncertainty on the X_{dca} of the track. Secondary vertices are selected by requiring the decay-length significance $L_{xy}/\sigma_{L_{xy}}$ to be greater than 7, where L_{xy} is the decay-length and $\sigma_{L_{xy}}$ is the estimated uncertainty on L_{xy}, calculated from the error matrices of the tracks and the primary vertex. Jets are considered tagged by this algorithm when a secondary vertex lies within a cone of $R = 0.5$ of the original jet axis.

IV. SELECTION RESULTS

We estimate the acceptances for s-channel and t-channel single top quark production using events generated by the CompHEP matrix element event generator [10]. We use both Monte Carlo and data to estimate the background yields. The W+jets and diboson (WW and WZ) backgrounds are estimated using Monte Carlo events generated with Alpgen [11]. The diboson background yield is normalized to NLO cross sections computed with MCFM [12]. The overall W+jets yield is normalized to the data sample before requiring a b-tagged jet, and the fraction of heavy-flavor ($Wb\bar{b}$) events is found using MCFM with the same parton-level cuts applied. This normalization to data also accounts for smaller contributions such as Z+jets events, where one of the leptons from the Z decay is not reconstructed. The $t\bar{t}$ background is estimated using Monte Carlo samples generated with Alpgen, normalized to the (N)NLO cross section calculation: $\sigma(t\bar{t}) = 6.7 \pm 1.2$ pb [13], where the uncertainty on the top quark mass is taken into account in the cross section uncertainty. The parton-level samples are then processed with Pythia [14] and a Geant [15]-based simulation of the DØ detector, and the resulting lepton and jet energies are smeared to reproduce the resolutions observed in data. The misidentified lepton background is estimated using multijet data samples that pass all event selection cuts but fail the electron likelihood requirement in the electron channel or the muon isolation requirement in the muon channel.

The acceptances for signal events with at least one b-tagged jet are $2.7 \pm 0.2\%$ and $1.9 \pm 0.2\%$ for the s-channel and t-channel respectively. The acceptance is calculated as the fraction of events that pass the selection. All possible single top decays, including all leptonic and hadronic decays of the W boson, are taken into account. Estimates for signal and background yields as well as the observed number of events after selection are shown in Table I.

	s-channel	t-channel
tb	5.5 ± 1.3	4.7 ± 1.0
tqb	8.6 ± 1.9	8.5 ± 1.9
$t\bar{t}$	78.3 ± 18.3	75.9 ± 17.6
W+jets	169.1 ± 20.1	163.9 ± 18.7
Mis-ID'd lepton	31.4 ± 3.3	31.3 ± 3.2
Background sum	287.4 ± 43.6	275.8 ± 40.6
Observed events	283	271

TABLE I: Estimates for signal and background yields and the numbers of observed events in data after event selection for the electron and muon, =1 tag and ≥2 tags analyses combined. The W+jets yields include the diboson backgrounds.

V. FINAL ANALYSIS

All three analysis methods start from the same set of discriminating variables, which fall into three categories: individual object kinematics, global event kinematics, and variables based on angular correlations. These variables are selected based on an analysis of Feynman diagrams of signals and backgrounds [16] and on a study of single top quark production at NLO [4]. The list of variables is shown in Table II. The variables are based on the following final state objects: the W boson reconstructed from the isolated lepton and the missing transverse energy. The z-component of the neutrino momentum is calculated using a W boson mass constraint, choosing the solution with smaller $|p_z^\nu|$ from the two possible solutions. Jets that have not been identified by the b-tagging algorithm are called "untagged" jets. The best jet is defined as the jet in each event for which the invariant mass of the system of reconstructed W boson and jet is closest to 175 GeV. In the s-channel analysis, the supposed top quark is reconstructed from the W boson and the best jet. In the t-channel analysis, the top quark is reconstructed from the W boson and the leading b-tagged jet.

A. Neural Networks

After event selection, neural networks are used to improve the signal-background separation. The networks are composed of three layers (input, hidden, output). For training and testing we use the MLPfit [17] package. Testing and training event sets are created by dividing signal and background Monte Carlo samples. To prevent overtraining, we used a technique called early stopping [18] to determine the maximum number of epochs for training. Each network is then tuned by choosing the optimal number of hidden nodes. From studies based on optimizing the expected limits on the single top quark cross sections, we find the two networks that are most effective in each channel. These networks correspond to the dominant backgrounds: $W + b\bar{b}$ and $t\bar{t} \to \ell$ + jets. Therefore, eight separate neural networks are used corresponding to the combinations of signal-background pairs ($tb - Wbb$, $tb - t\bar{t}$, $tqb - Wbb$, $tqb - t\bar{t}$) and lepton flavors (electron or muon). The input variables to each network are selected by training with different combinations

		Signal-Background Pairs			
		tb		tqb	
		Wbb	$t\bar{t}$	Wbb	$t\bar{t}$
	Individual object kinematics				
$p_T(\text{jet1}_{\text{tagged}})$	Transverse energy of the leading tagged jet	√	√	√	—
$p_T(\text{jet1}_{\text{untagged}})$	Transverse energy of the leading untagged jet	—	—	√	√
$p_T(\text{jet2}_{\text{untagged}})$	Transverse energy of the second untagged jet	—	—	—	√
$p_T(\text{jet1}_{\text{nonbest}})$	Transverse energy of the leading nonbest jet	√	√	—	—
$p_T(\text{jet2}_{\text{nonbest}})$	Transverse energy of the second nonbest jet	√	√	—	—
	Global event kinematics				
$M_T(\text{jet1}, \text{jet2})$	Transverse mass of the leading-two-jets system	√	—	—	—
$p_T(\text{jet1}, \text{jet2})$	Transverse momentum of the leading-two-jets system	√	—	√	—
$M(\text{alljets})$	Invariant mass of the all-jets system	√	√	√	√
$H_T(\text{alljets})$	Sum of the transverse energies of all jets	—	—	√	—
$M(\text{alljets} - \text{jet1}_{\text{tagged}})$	Invariant mass of the all-jets system, excluding the leading tagged jet	—	—	—	√
$H(\text{alljets} - \text{jet1}_{\text{tagged}})$	Total energy of all jets except the leading tagged jet	—	√	—	√
$H_T(\text{alljets} - \text{jet1}_{\text{tagged}})$	Total transverse energy of all jets, excluding the leading tagged jet	—	—	—	√
$p_T(\text{alljets} - \text{jet1}_{\text{tagged}})$	Transverse momentum of the all-jets system, excluding the leading tagged jet	—	√	—	√
$M(\text{alljets} - \text{jet}_{\text{best}})$	Invariant mass of the all-jets system, excluding the best jet	—	√	—	—
$H(\text{alljets} - \text{jet}_{\text{best}})$	Total energy of all jets except the best jet	—	√	—	—
$H_T(\text{alljets} - \text{jet}_{\text{best}})$	Total transverse energy of all jets except the best jet	—	√	—	—
$M(\text{top}_{\text{tagged}}) = M(W, \text{jet1}_{\text{tagged}})$	Invariant mass of the reconstructed top quark using the leading tagged jet	√	√	√	√
$M(\text{top}_{\text{best}}) = M(W, \text{jet}_{\text{best}})$	Invariant mass of the reconstructed top quark using the best jet	√	—	—	—
$\sqrt{\hat{s}}$	Invariant mass of the final state system	√	—	√	√
	Angular variables				
$\Delta R(\text{jet1}, \text{jet2})$	Angular separation between the leading two jets	√	—	√	—
$Q(\text{lepton}) \times \eta(\text{jet1}_{\text{untagged}})$	Pseudorapidity of the leading untagged jet $\times$ lepton charge	—	—	√	√
$\cos(\text{lepton}, Q(\text{lepton}) \times z)_{\text{top}_{\text{best}}}$	Top quark spin in the s-channel in the optimal basis, reconstructing the top quark with the best jet	√	—	—	—
$\cos(\text{lepton}, \text{jet1}_{\text{untagged}})_{\text{top}_{\text{tagged}}}$	Top quark spin in the optimal basis in the t-channel, reconstructing the top quark with the leading tagged jet	—	—	√	—
$\cos(\text{alljets}, \text{jet1}_{\text{tagged}})_{\text{alljets}}$	Cosine of the angle between the leading tagged jet and the all-jets system in the all-jets rest frame	—	—	√	√
$\cos(\text{alljets}, \text{jet}_{\text{nonbest}})_{\text{all jets}}$	Cosine of the angle between the leading non-best jet and the all-jets system in the all-jets rest frame	—	√	—	—

TABLE II: Discriminant variables used as input for the three analysis methods. The columns show which variables are used in each signal-background pair in the neural network and decision tree analyses.

of variables and choosing the combination that produces the minimum testing error. Table II shows which variables are used in each signal-background pair. Since the discriminating variables do not depend on the lepton kinematics, the electron and muon analyses share the same input variables.

Figure 1 shows a comparison of background, signal, and data for the jet multiplicity and several discriminating variables that show good signal-background separation. It can be seen that the background model reproduces the data well in all distributions.

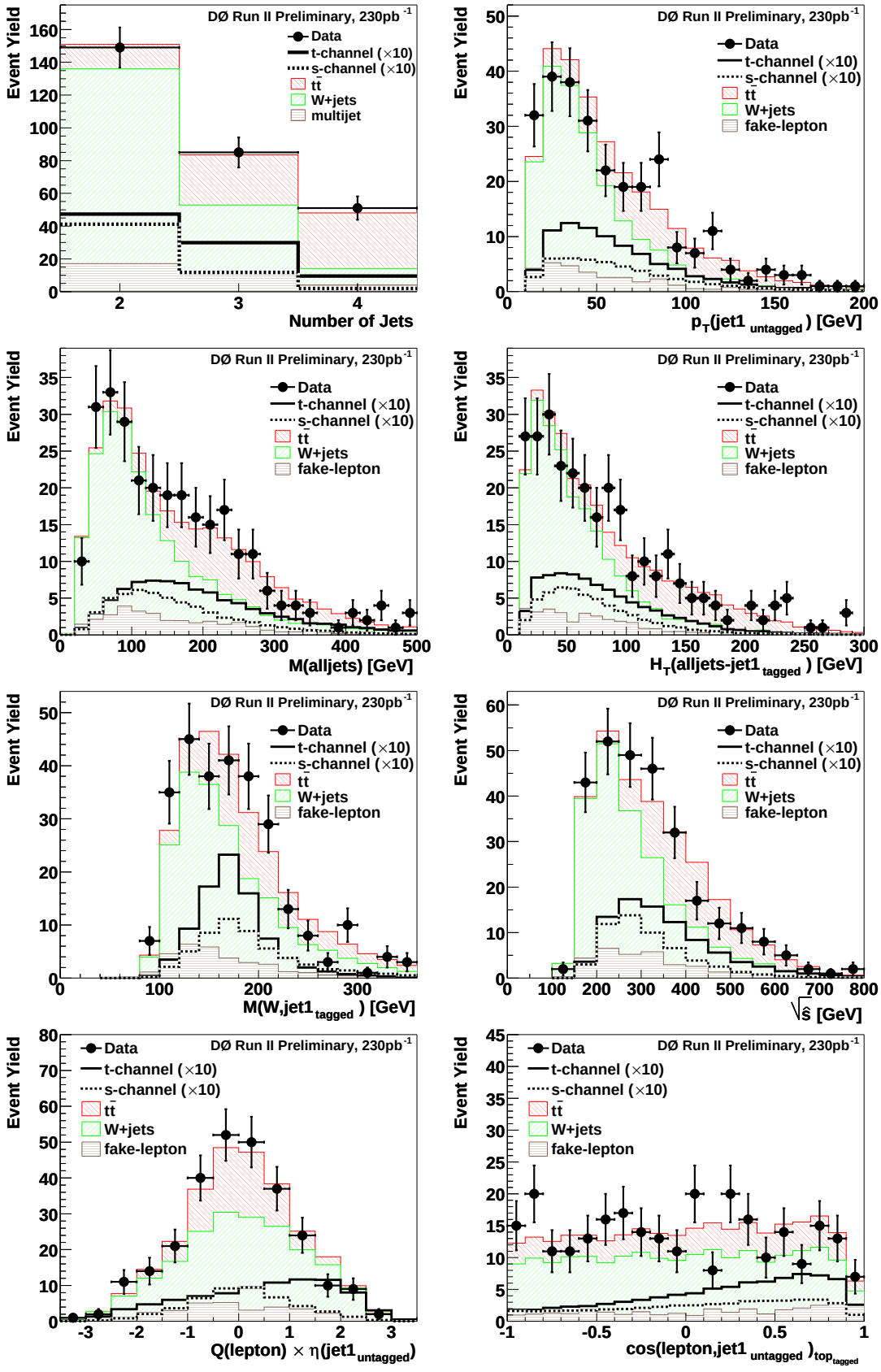

FIG. 1: Data-background comparison for the jet multiplicity distribution and seven of the important neural network and decision tree input variables, for the electron and muon channels combined, requiring at least one tag.

The performance of the neural networks is illustrated in Fig. 2, where the output of four of the eight neural networks is displayed for the corresponding signal-background pairs used in their training. The networks separate signal and $t\bar{t}$ backgrounds efficiently, but give less separation for W+jets, especially in the s-channel. Figure 3 shows the outputs of the eight neural networks for comparison between the data and the expected backgrounds and signals.

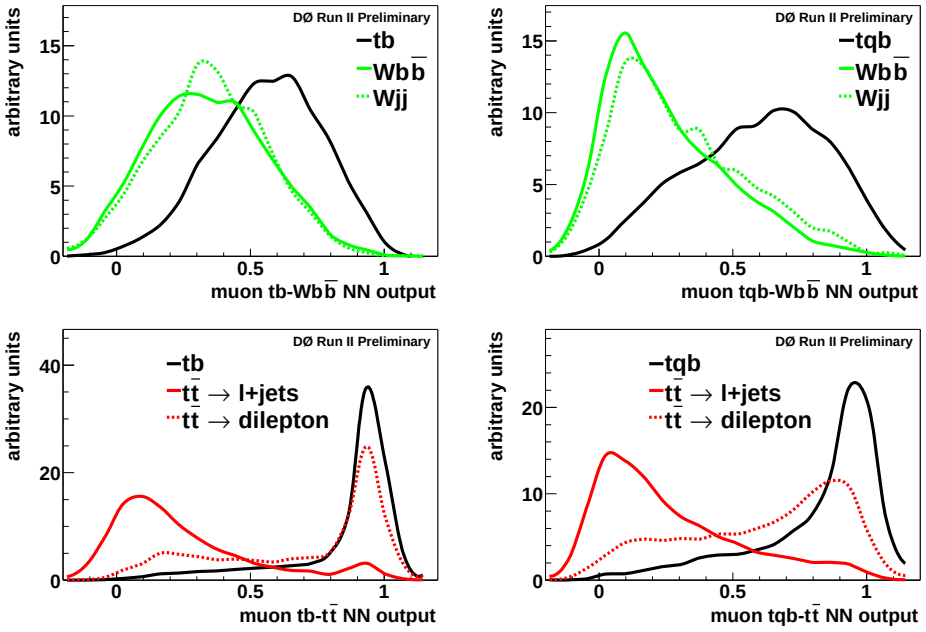

FIG. 2: Outputs of the four neural networks in the muon channel. The upper row shows the Wbb outputs, the lower row the $t\bar{t}$ outputs. The left column shows the s-channel outputs and the right column the t-channel outputs. Wjj is W+jets Monte Carlo where $j = g, u, d, s$ or c partons. The electron analysis networks have similar performance.

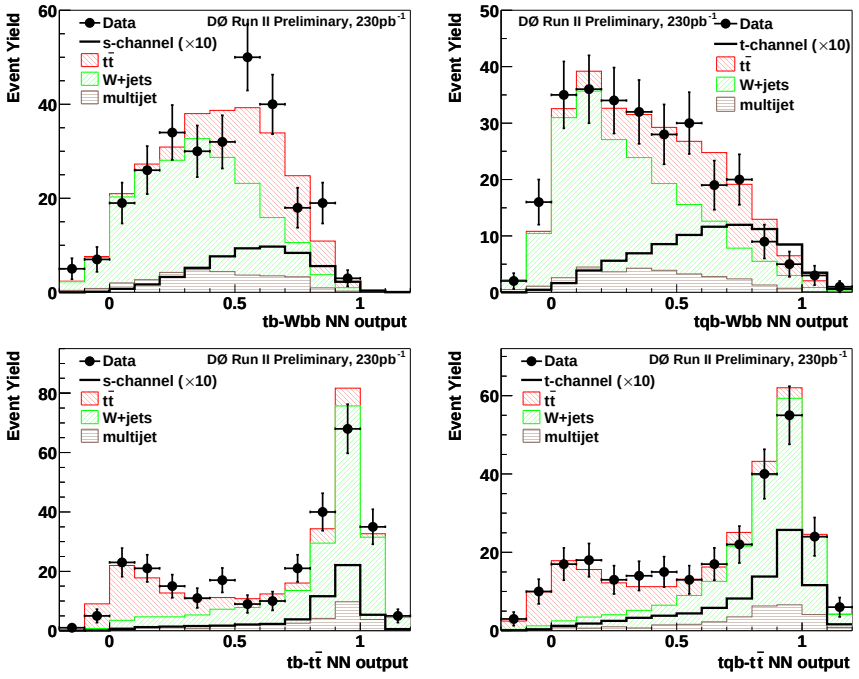

FIG. 3: Comparison of background, signal, and data for the neural network outputs, for the electron and muon channels combined, requiring at least one tag. The upper row shows the Wbb outputs, the lower row the $t\bar{t}$ outputs. The left column shows the s-channel outputs and the right column the t-channel outputs. Signals are multiplied by 10 for readability.

B. Decision Trees

We have also used decision trees to evaluate the probability that a given event is a signal event. A decision tree is a binary tree with a simple selection cut implemented at each node [19]. Each event follows a unique path through the tree until it ends in one of the leaves. Each of these leaves is represented by a purity value, which is the ratio of signal and background events from the training samples that end up in this particular leaf. The distribution of purity values determines the decision tree output. The tree is trained using a procedure similar to the optimization of a neural network. We use the same input variables and the same number of decision trees as in the neural network analysis. The performance of the decision trees is shown in Fig. 4, where the output of the decision tree is displayed for the corresponding signal-background pairs used in their training. The decision trees separate signal and $t\bar{t}$ backgrounds efficiently, but give less separation for W+jets, especially in the s-channel. Figure 5 shows a comparison of the outputs of the decision trees between data, expected backgrounds, and signals. The discrete nature of the distributions is a function of the number of nodes and the discrete nature of the decision trees.

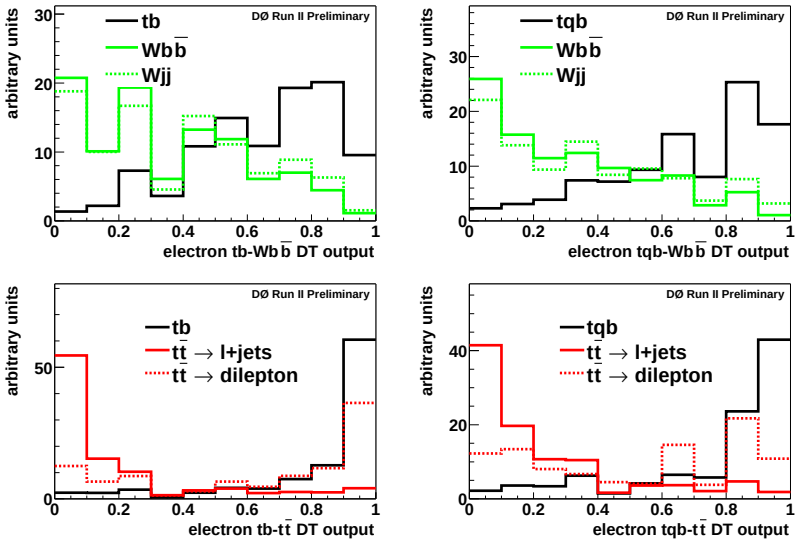

FIG. 4: Outputs of the four decision trees in the electron channel. Wjj is W+jets Monte Carlo where $j = g, u, d, s$ or c partons. The muon analysis decision trees have similar performance.

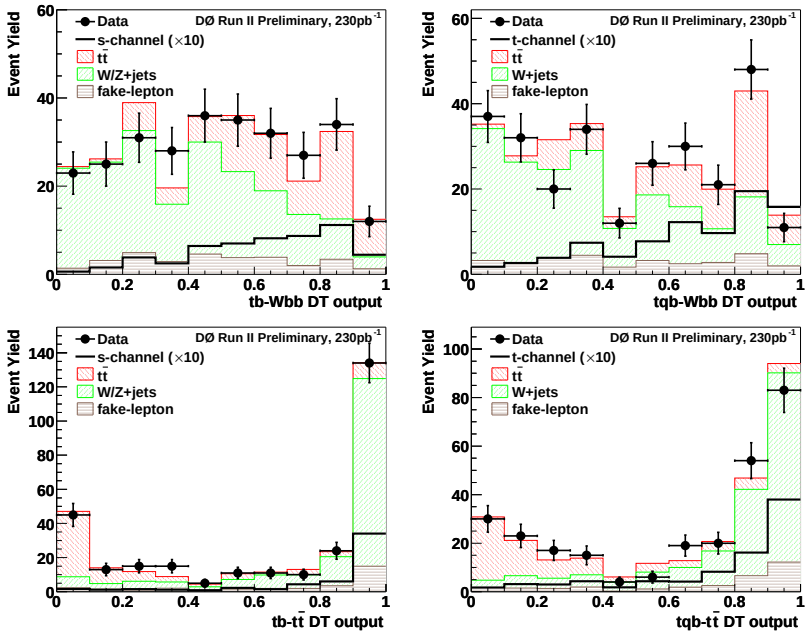

FIG. 5: Comparison of background, signal, and data for the decision tree outputs, for the electron and muon channels combined, requiring at least one tag. The upper row shows the Wbb outputs, the lower row the $t\bar{t}$ outputs. The left column shows the s-channel outputs and the right column the t-channel outputs. Signals are multiplied by 10 for readability.

C. Cut-Based Analysis

In parallel to multivariate techniques like neural networks and decision trees, a set of sequential cuts on the variables listed in Table II has also been performed. First, each variable is rated according to the best expected limit that an optimal cut on that single variable would achieve for each channel. The method used to choose the optimal cut point uses the signal events to seed the cut values and minimizes the expected limit. Then, once each channel has the most effective variables identified, they are combined (ANDed) in order, and for each subset the optimal cut values are recalculated. The set of variables and their optimized cuts that yields the lowest expected limit is then chosen for that particular channel.

Table III shows the optimal variable sets and cuts found for each channel. Table IV shows the numbers of events and expected background and signal yields after these cuts have been applied.

	s-channel		t-channel	
Channel	Variables	Cuts	Variables	Cuts
Electron				
=1 Tag	$p_T(\text{jet1}_{\text{tagged}})$	> 27 GeV	$H_T(\text{alljets})$	> 71 GeV
	$M(\text{alljets} - \text{jet1}_{\text{tagged}})$	< 70 GeV	$M(\text{alljets})$	> 57 GeV
	$\sqrt{\hat{s}}$	> 196 GeV	$\sqrt{\hat{s}}$	> 203 GeV
			$\lvert 175 - M(\text{top}_{\text{tagged}})\rvert$	< 57 GeV
			$p_T(\text{jet1}_{\text{tagged}})$	> 21 GeV
$\geq$2 Tags	$p_T(\text{jet1}_{\text{tagged}})$	> 42 GeV	$p_T(\text{jet1}_{\text{tagged}})$	> 34 GeV
	$M(\text{alljets} - \text{jet1}_{\text{tagged}})$	< 98 GeV	$M(\text{alljets} - \text{jet1}_{\text{tagged}})$	< 75 GeV
	$H(\text{alljets} - \text{jet}_{\text{best}})$	< 304 GeV	$H(\text{alljets} - \text{jet1}_{\text{tagged}})$	< 504 GeV
	$H(\text{alljets} - \text{jet1}_{\text{tagged}})$	< 304 GeV	$H(\text{alljets} - \text{jet}_{\text{best}})$	< 504 GeV
Muon				
=1 Tag	$p_T(\text{jet1}_{\text{tagged}})$	> 33 GeV	$\lvert 175 - M(\text{top}_{\text{tagged}})\rvert$	< 60 GeV
	$M(\text{alljets} - \text{jet1}_{\text{tagged}})$	< 74 GeV	$\sqrt{\hat{s}}$	> 210 GeV
	$H(\text{alljets} - \text{jet}_{\text{best}})$	< 504 GeV	$M(\text{alljets})$	> 70 GeV
	$H(\text{alljets} - \text{jet1}_{\text{tagged}})$	< 504 GeV	$H_T(\text{alljets})$	> 58 GeV
$\geq$2 Tags	$p_T(\text{jet1}_{\text{tagged}})$	> 33 GeV	$\lvert 175 - M(\text{top}_{\text{tagged}})\rvert$	< 213 GeV
	$M(\text{alljets} - \text{jet1}_{\text{tagged}})$	< 74 GeV		
	$H(\text{alljets} - \text{jet}_{\text{best}})$	< 504 GeV		
	$H(\text{alljets} - \text{jet1}_{\text{tagged}})$	< 504 GeV		

TABLE III: The best set of variables and cuts for each channel in the cut-based analysis. The variables are defined in Table II.

	s-channel	t-channel
tb	4.5 ± 1.0	3.2 ± 0.8
tqb	5.5 ± 1.2	7.0 ± 1.6
$t\bar{t}$	27.6 ± 7.6	55.9 ± 12.3
W+jets	102.9 ± 13.7	72.6 ± 9.7
Mis-ID'd lepton	17.2 ± 2.0	17.0 ± 2.0
Background sum	153.1 ± 24.5	148.7 ± 24.8
Observed events	152	148

TABLE IV: Estimates of background and signal yields and the number of observed events in data after the cut-based selection for the electron and muon, =1 tag and $\geq$2 tags analyses combined.

VI. SYSTEMATIC UNCERTAINTIES

Systematic uncertainties are evaluated for the Monte Carlo signal and background samples, separately for electrons and muons and for each b-tag multiplicity. The dominant sources of systematic uncertainty on the signal and background acceptances are (a) 8% uncertainty on the b-tag modeling in the Monte Carlo, (b) 8% uncertainty from the jet energy scale, (c) 5% uncertainty on the object identification efficiency, (d) 5% uncertainty on the trigger modeling, and (e) 5% uncertainty on the modeling of jet fragmentation. Each of these systematic uncertainties has been evaluated by varying the uncertainty for each object in the event (electrons, muons, jets) up and down by one standard deviation, and then propagating the updated objects and corresponding weights through the analysis chain. The uncertainty on the integrated luminosity is 6.5% [20]. The background yields also have an uncertainty from the cross section, which varies from 8% for diboson production to 18% for the $t\bar{t}$ samples [13]. Since the W+jets background is normalized to the data before tagging, the yield estimate is only affected by uncertainties related to b-tagging. These include the b-tag modeling uncertainty, and the uncertainty in the flavor composition before tagging, which is estimated at 25%. The uncertainties from b-tag modeling and the jet energy scale are higher when requiring at least two tagged jets. The total uncertainty on the signal acceptance for single-tagged events is 13% for the s-channel and 15% for the t-channel, and for double-tagged events it is 24% for the s-channel and 28% for the t-channel. The total uncertainty on the background is 10% for the single-tagged samples and 26% for the double-tagged samples.

VII. CROSS SECTION LIMITS

The observed data are consistent with the background predictions for the three analysis methods and all eight analysis channels within uncertainties. We therefore set upper limits on the s-channel and t-channel production cross sections using a Bayesian approach [21]. For the cut-based analysis, the inputs to the limit calculation are the integrated luminosity and the predicted and observed yields. For the neural network and decision tree analyses, we use the two-dimensional distributions of the Wbb vs $t\bar{t}$ filter outputs. We assume a Poisson distribution for the observed counts, and a flat prior probability for the signal cross section. The priors for the signal acceptance and the background yields are multivariate Gaussians centered on their estimates and described by a covariance uncertainty matrix taking into account correlations across the different sources and bins.

We combine the single-tagged and double-tagged analysis channels, as well as the electron and muon channels, to obtain better sensitivity to the single top cross sections. Plots of the Bayesian posterior probability density as a function of the single top cross section from the cut-based, decision tree, and neural network analyses are shown in Fig. 6, for both the s-channel and t-channel searches. The corresponding limits at 95% confidence level are 6.4 pb in the s-channel and 5.0 pb in the t-channel from the neural networks analysis; 8.3 pb in the s-channel and 8.1 pb in the t-channel from the decision trees analysis; and 10.6 pb in the s-channel and 11.3 pb in the t-channel from the cut-based analysis. The expected limits from the neural network (decision tree, cut-based) analysis are 4.5 pb (4.5 pb, 9.8 pb) in the s-channel and 5.8 pb (6.4 pb, 12.4 pb) in the t-channel. The improvement in limits from the cut-based analysis to the neural network and decision tree analyses comes from both the use of multivariate techniques that take into account correlations in the data, and from the binned likelihood fits, which add shape information from the distributions.

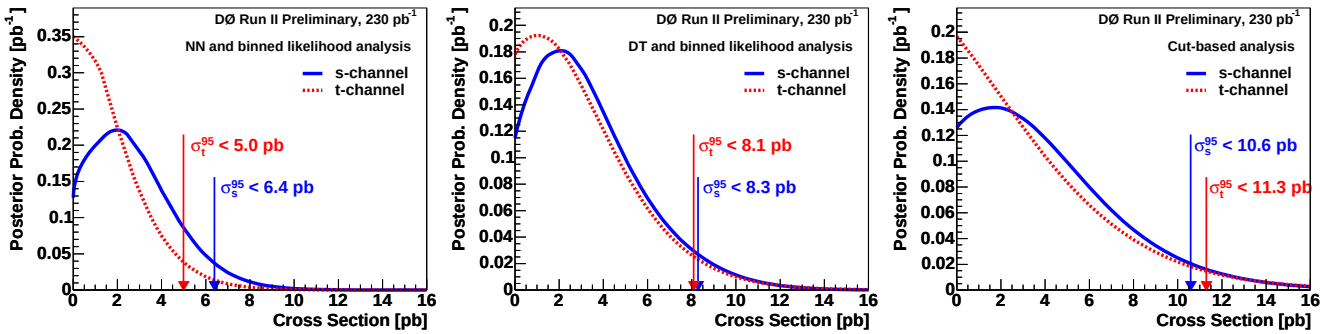

FIG. 6: The Bayesian posterior densities for the neural networks analysis (left), decision trees analysis (center), and the cut-based analysis (right).

VIII. SUMMARY

No evidence is found for electroweak production of single top quarks in 230 pb^{-1} of data collected with the DØ detector at $\sqrt{s} = 1.96$ TeV. A secondary-vertex reconstruction algorithm has been employed to select events with exactly one or more than one b jet in electron+jets and muon+jets final states. Upper limits at the 95% confidence level on the cross section for the s-channel and t-channel processes have been set using binned likelihood fits to the output variables from neural networks and decision trees, and using event counts in the cut-based analysis. The s-channel limit of 6.4 pb and the t-channel limit of 5.0 pb are significant improvements over previously published limits [5–8]. They are also close to the region of sensitivity to models of physics beyond the standard model, such as a fourth quark generation scenario with large $|V_{ts}|$, or a flavor-changing neutral-current vertex [22], as shown in Fig. 7.

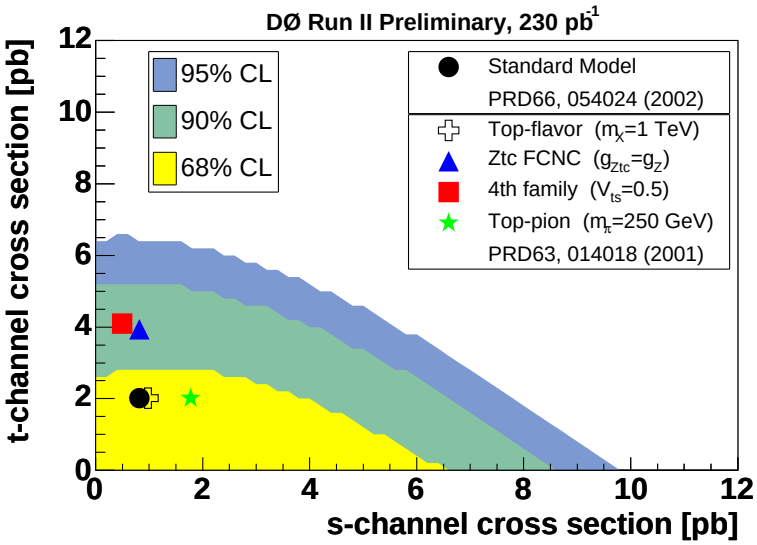

FIG. 7: Exclusion contours at 68%, 90%, and 95% confidence level on the posterior density distribution as a function of both the s-channel and t-channel cross sections in the neural networks analysis. The s-channel cross section is obtained from tb muon data only and the t-channel cross section from tqb electron channel data only, such that the two likelihoods are independent. Several representative non-standard model contributions from Ref. [22] are also shown.

Acknowledgements

We thank the staffs at Fermilab and collaborating institutions, and acknowledge support from the Department of Energy and National Science Foundation (USA), Commissariat à l'Energie Atomique and CNRS/Institut National de Physique Nucléaire et de Physique des Particules (France), Ministry of Education and Science, Agency for Atomic Energy and RF President Grants Program (Russia), CAPES, CNPq, FAPERJ, FAPESP and FUNDUNESP (Brazil), Departments of Atomic Energy and Science and Technology (India), Colciencias (Colombia), CONACyT (Mexico), KRF (Korea), CONICET and UBACyT (Argentina), The Foundation for Fundamental Research on Matter (The Netherlands), PPARC (United Kingdom), Ministry of Education (Czech Republic), Canada Research Chairs Program, CFI, Natural Sciences and Engineering Research Council and WestGrid Project (Canada), BMBF and DFG (Germany), Science Foundation Ireland, A.P. Sloan Foundation, Research Corporation, Texas Advanced Research Program, and the Alexander von Humboldt Foundation.

[1] F. Abe *et al.*, (CDF Collaboration), "Observation of Top Quark Production in $p\bar{p}$ Collisions," Phys. Rev. Lett. **74**, 2626 (1995); S. Abachi *et al.*, (DØ Collaboration), "Observation of the Top Quark," Phys. Rev. Lett. **74**, 2632 (1995).

[2] B.W. Harris, E. Laenen, L. Phaf, Z. Sullivan, and S. Weinzierl, "Fully Differential Single-Top-Quark Cross Section in Next-to-Leading Order QCD," Phys. Rev. D **66**, 054024 (2002); Z. Sullivan, "Understanding Single-Top-Quark Production and Jets at Hadron Colliders," to appear in Phys. Rev. D, hep-ph/0408049.

[3] J. Campbell, R. K. Ellis and F. Tramontano, "Single Top Production and Decay at Next-to-Leading Order," Phys. Rev. D **70**, 094012 (2004).

[4] Q.-H. Cao, R. Schwienhorst, and C.-P. Yuan, "Next-to-Leading Order Corrections to Single Top Quark Production and Decay at the Tevatron: 1: s-channel process," to appear in Phys. Rev. D, hep-ph/0409040 (2004).

[5] B. Abbott *et al.*, (DØ Collaboration), "Search for Electroweak Production of Single Top Quarks in $p\bar{p}$ Collisions," Phys. Rev. D **63**, 031101 (2001).

[6] V.M. Abazov *et al.*, (DØ Collaboration), "Search for Single Top Quark Production at DØ Using Neural Networks," Phys. Lett. **B517**, 282 (2001).

[7] D. Acosta *et al.*, (CDF Collaboration), "Search for Single Top Quark Production in $p\bar{p}$ Collisions at $\sqrt{s} = 1.8$ TeV," Phys. Rev. D **65**, 091102 (2002).

[8] D. Acosta *et al.*, (CDF Collaboration), "Search for Electroweak Single-Top-Quark Production in $p\overline{p}$ Collisions at $\sqrt{s} = 1.96$ TeV" Phys. Rev. D **71**, 012005 (2005),

[9] V. Abazov *et al.*, DØ Collaboration, in preparation for submission to Nucl. Instrum. Methods in Phys. Res. **A**; T. LeCompte and H.T. Diehl, Ann. Rev. Nucl. Part. Sci. **50**, 71 (2000).

[10] E. Boos *et al.*, (CompHEP Collaboration), "CompHEP 4.4: Automatic Computations from Lagrangians to Events," Nucl. Instrum. Meth. A **534**, 250 (2004);
E.E. Boos, L.V. Dudko, and V.I. Savrin, "'SingleTop' — an Event Generator for the Single Top Quark Production at the LHC," CMSNote 2000/065.

[11] M.L. Mangano, M. Moretti, F. Piccinini, R. Pittau, and A.D. Polosa, "ALPGEN v1.3, a Generator for Hard Multiparton Processes in Hadronic Collisions," J. High Energy Physics **0307**, 001 (2003).

[12] J. Campbell and K. Ellis, "MCFM Monte Carlo for FeMtobarn Processes"; `http://mcfm.fnal.gov`; J. Campbell and K. Ellis, Next-to-Leading Order Corrections to W+2 Jet and Z+2 Jet Production at Hadron Colliders, hep-ph/0202176.

[13] N. Kidonakis and R. Vogt, "Next-to-Next-to-Leading Order Soft-Gluon Corrections in Top Quark Hadroproduction," Phys. Rev. D **68**, 114014 (2003).

[14] T. Sjöstrand *et al.*, "PYTHIA 6.2: Physics and Manual," hep-ph/0108264.

[15] R. Brun *et al.*, "GEANT - Detector Description and Simulation," CERN Program Library Long Writeup W 5013 (1994).

[16] L. Dudko, for the DØ Collaboration, "Use of Neural Networks in a Search for Single Top Quark Production at DØ ," in the proceedings of the 7th International Workshop on Advanced Computing and Analysis Techniques in Physics Research, Fermilab, Batavia, IL, (October 2000); E. Boos and L. Dudko, "Optimized Neural Networks to Search for Higgs Boson Production at the Tevatron," Nucl. Instrum. Methods **A 502**, 486 (2003).

[17] J. Schwindling, "MLPfit: A Tool For Designing and Using Multi-Layer Perceptrons," `http://schwind.home.cern.ch/schwind/MLPfit.html`.

[18] G. Orr and K. Müller, "Neural Networks: Tricks of the Trade," Springer-Verlag, Berlin, 55 (1998).

[19] L. Breiman, J. Friedman, R. Olshen, and C. Stone, "Classification and Regression Trees," Wadsworth (1984).

[20] T. Edwards *et al.* (DØ Collaboration), "Determination of the Effective Inelastic $p\bar{p}$ Cross-Section for the DØ Run II Luminosity Measurement," FERMILAB-TM-2278-E (2004).

[21] I. Bertram et al., "A Recipe for the Construction of Confidence Limits," Fermilab-TM-2104 (2000).

[22] T. Tait and C. P. Yuan, "Single Top Quark Production as a Window to Physics Beyond the Standard Model," Phys. Rev. D **63**, 014018 (2001).